

# Journal of Advanced Research in Fluid Mechanics and Thermal Sciences



Journal homepage: https://semarakilmu.com.my/journals/index.php/fluid\_mechanics\_thermal\_sciences/index ISSN: 2289-7879

# Comparative Analysis of Flow Dynamics Studies between the Straight and Interrupted Minichannel Heat Sink

Ernie Mat Tokit<sup>1,2,\*</sup>, Mohd Zamri Yusoff<sup>3</sup>, Safarudin Gazali Herawan<sup>4</sup>

- <sup>1</sup> Fakulti Teknologi dan Kejuruteraan Mekanikal, Universiti Teknikal Malaysia Melaka, 76100 Durian Tunggal, Melaka, Malaysia
- Centre for Advanced Research on Energy, Universiti Teknikal Malaysia Melaka, 76100 Durian Tunggal, Melaka, Malaysia
- <sup>3</sup> Department of Mechanical Engineering, College of Engineering, Universiti Tenaga Nasional, 43000 Kajang, Selangor, Malaysia
- Industrial Engineering, Faculty of Engineering, Bina Nusantara University, Jakarta, 11480 Indonesia

#### **ARTICLE INFO**

#### **ABSTRACT**

#### Article history:

Received 5 January 2025 Received in revised form 7 April 2025 Accepted 15 April 2025 Available online 30 April 2025

## A simulation work was performed to investigate the advantage of interrupted minichannel heat sink over the straight one in terms of flow dynamics. Four different designs were examined, namely i) a straight, ii) Design A, iii) Design B and iv) Design C minichannel. All channels were rectangular in cross sectional area with 0.0032 m of hydraulic diameter, having cuts in between. Parametric studies were performed by utilizing the propylene glycol as the coolant fluid, while the Reynolds number are diverse between 510.9 to 608.2. The flow is modelled as steady and 3D flow. Comparative analysis between simulated and experimental data was first conducted as validation purposes with deviation of 0.49% to 9.81%, and 1.08% to 12.48% for $P_{drop}$ and Nusselt number respectively. The predicted results depicted the design features that affect the flow behaviours such as sharp corner edge that diminish Coanda effect and promotes flow separation, reverse flow and recirculation zone, and interrupts boundary layer. These behaviour causes the increment of heat flux and $(T_{out}-T_{in})/(T_w-T_m)$ , while decrement in wall shear stress that finally augment the heat transfer. Comparative analysis showed that the increment in heat flux by 26.3% to 33.3%, $(T_{out}-T_{in})/(T_w-T_m)$ by 25% to 42.8%, and decrement in wall shear stress by 25% to 35.7%, indicating improved flow characteristics.

#### Keywords:

Microchannel heat sink; interrupted; redeveloping boundary layer; flow dynamics

## 1. Introduction

A small-size-channel heat sink is a unique channel design used to offer superior heat dissipation. The channel's size can be categorized according to the hydraulic diameter, as summarized in Figure 1, from nanoscale to macroscale. Its smaller dimension in hydraulic diameter promotes a higher surface-to-volume ratio while increasing the contact surface of the microchannel's wall with the coolant fluid. As more contact surface is formed, the heat transfer can be swiftly removed from the channel's wall and carried away by the coolant fluid. This causes a higher temperature difference between the heat source and the fluid, which is an indicator of the enhancement in heat transfer rate.

E-mail address: ernie@utem.edu.my

https://doi.org/10.37934/arfmts.130.2.196214

<sup>\*</sup> Corresponding author.

The fluid dynamics of the flow behaves the same generally for all channel size, except for some parameters which are more pronounced as the hydraulic diameter becomes smaller. As the fluid flows through the channel, the velocity decreases along the flow due to the wall and fluid friction, and the viscosity of the fluid itself. The surface roughness generates more friction that causes the flow to rotate and overlap each other [1]. The heat transfer can be extended by introducing the flow interrupter such as wavy or curvy wall, obstacles like ribs, fins, or baffles within the channels [2,3]. These obstructions force the fluid to flow around them, breaking up the stagnant layer and promoting turbulence. Additionally, sudden changes in channel width, such as expansions or contractions, or interruption disrupts the Coanda effect or fluid's cling to the channel's surface that causes flow separation and detachment from the channel's wall, leading to boundary layer redevelopment [4]. The disruption results in a thinner thermal boundary layer, reducing the overall thermal resistance and improving heat transfer [5]. This thermal boundary layer is the thin layer of fluid near the heated surface wall where the fluid's temperature changes rapidly from the surface temperature to the bulk fluid temperature.

Since the study of flow in microchannel are huge as compared to minichannel's flow, some flow dynamics of microchannel's flow are being reviewed here to support the data of minichannel flow behaviour. Among other approaches of heat transfer augmentation method is utilizing wavy or twisted channels. These curved walls induce secondary flows within the fluid, further disrupting the boundary layer and enhancing heat transfer [6,7]. In addition to that, any interruption to flow causes rapid changes in velocity and increases the velocity gradient. This directly causes the growth of wall shear stress after each interruption but decreases along the channel [8,9]. Any sharp edges cause the fluid to precede the wall's shape and recirculate to form a recirculation zone with nearly low velocity to stagnant flow at the centre of the circulation flow [10]. The vortex boundary is developed as a separator between the recirculation zone and the core fluid region. However, the vortex is not strong enough without any driving force, and the flow separation diffuses with a blurred vortex boundary. The core region that has higher velocity after sudden expansion also generates more velocity gradient that grows the wall shear stress. Moreover, a higher velocity gradient affects the higher heat flux that energizes the force to heat transfer enhancement.

All the flow dynamics that occur in the microchannel flow have been extensively investigated by utilizing numerical and experimental approaches in various parametric studies, including aspect ratio, coolant types, and microchannel configurations at diverse applications [11-14]. Straight channel designs are paid less attention nowadays except for their benefits in easier manufacturing and less cost. Meanwhile, numerous microchannel configurations, as shown in Figure 2, had been approached to boost the heat transfer and had been reviewed by several researchers in the past [15-19].

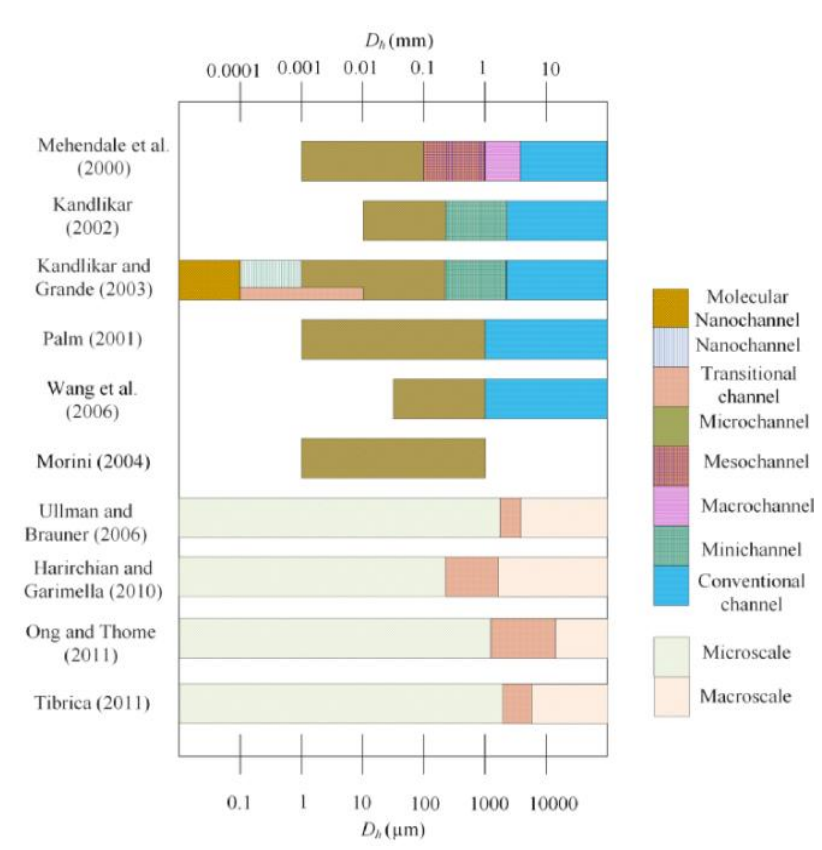
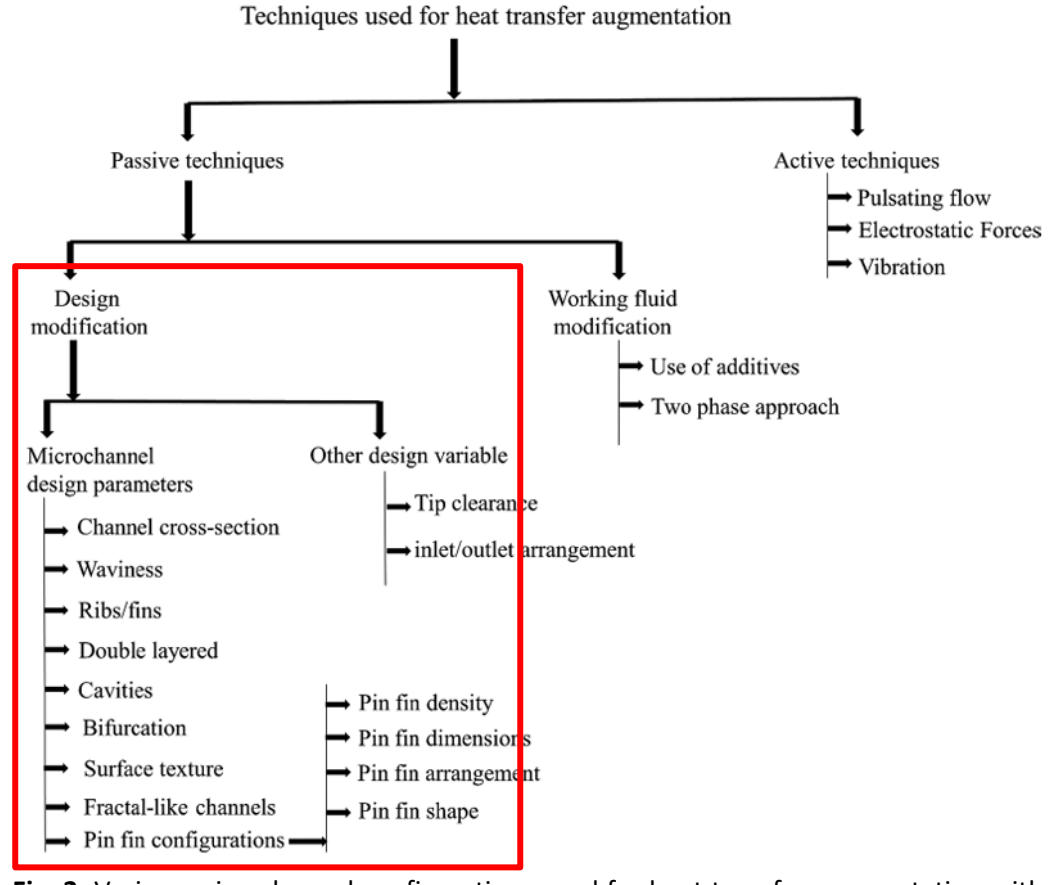


Fig. 1. Category of macroscale to nanoscale channel size [15]



**Fig. 2.** Various microchannel configurations used for heat transfer augmentation with the highlighted area being focused on in this study [15]

While existing research has explored boundary layer interruption techniques in microchannel heat sinks, several gaps remain. These include a limited understanding of the flow dynamics passing through the curving areas, obstacles, interruption, or any minichannel configuration as mentioned previously. All these shapes directly affect the flow dynamics in terms of the fluid velocity, temperature, wall shear stress, and wall heat flux that either promotes or inhibits the heat transfer growth. The integration between all these is presented in the discussion part. Hence, this study significantly addressed this understanding to further modify the minichannel heat sink design to augment the heat dissipation for cooling purposes.

# 2. Methodology

This section explains in detail the procedure of the simulation work that is methodically conducted.

#### 2.1 Model Details

There are 4 designs of the minichannels: straight, Design A, Design B, and Design C minichannels, as shown in Figure 3. Design A to C consists of cuts in between the straight channel, known as an interrupted minichannel. Figure 4 shows the view of interrupted minichannel that consists of 11 channels with height,  $H_{ch}$  of 8 mm and a width,  $W_{ch}$  of 2 mm while the total length,  $L_{ch}$  is 50 mm. The cut's length,  $L_c$  is 2 mm. The detail dimension is shown in Table 1. There are two-semi circle manifolds at both sides of the heat sink and the fluid coolant flows in and out vertically. The bottom surface is heated with constant heat flux. The top part of the heat sink is attached with pyrex and the other walls are assumed to be adiabatic. In order to solve the Navier-Stokes and energy equations, the following assumptions are made: i) the flow is assumed to be in a steady state and three-dimensional, ii) the flow is homogeneous and laminar, and iii) the properties of the fluid and solid are taken to be constant.

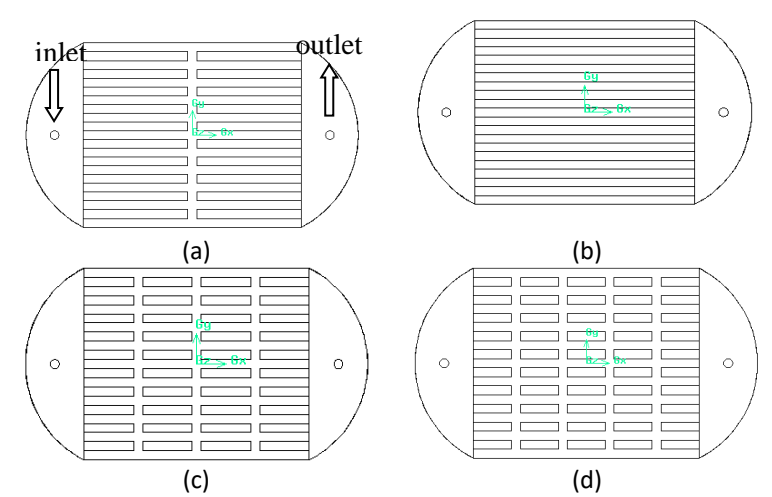


**Fig. 3.** Top view of the (a) straight and (b) design A, (c) design B and (d) design C microchannel heat sink

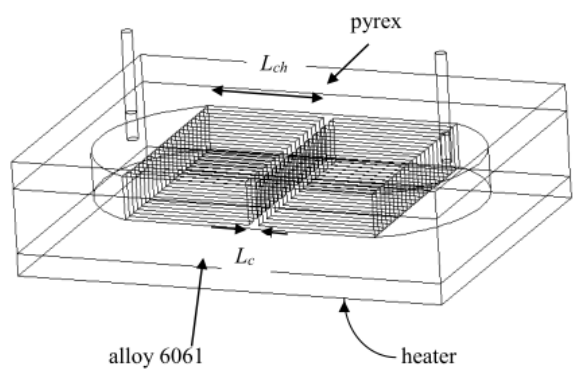


**Fig. 4.** Outer view of aluminum alloy-Design A heat sink with pyrex on the top and flat heater attached at the bottom of the heat sink

**Table 1**Dimensions of the rectangular minichannel heat sink

Design	Cut number,	Channel's length,	Length ratio,
Design	Cut Hulliber,	•	
	n	$L_{ch}$ (mm)	Lc/Lch
Straight	0	50	0
Α	2	48	0.0417
В	6	44	0.5455
С	8	34	0.238095

#### 2.2 Numerical Modeling

The finite volume method is used for modeling the fluid flow and heat transfer in interrupted minichannel heat sink. During pre-processing, the whole domain includes the fluid and solid domain are defined. The volume occupied by both the fluid and solid are divided into grids or meshes. The structured meshes are used to suit the computer's memory allocation and to obtain possible time to avoid expensive computational time. The mesh sizes are varied and the most suitable mesh are selected whereby the Nusselt number is no longer changing due to grid size variation. The Nusselt number represents the ratio of convective to conductive heat transfer. It shows the effectiveness of convection to the conduction alone. The physical models and boundary conditions are then defined. All the governing equations are solved iteratively as a steady-state flow. The partial differential equations are discretized using Finite Volume Method (FVM) and thermal parameters are calculated at each of the nodes. The standard SIMPLE algorithm is used to solve the pressure equation. The first order upwind scheme is used for both the momentum and energy conservation equations.

# 2.3 Single Phase Model Governing Equations

The governing equations are a set of equations used to model the behavior of fluid flow and thermal flow in the minichannel heat sink. The governing equations for mass, momentum, and energy, and also the heat diffusion in solid domain as displayed in Eq. (1) to Eq. (5), and Eq. (6) for the whole domain are used to predict the velocity, pressure and temperature profile, and heat transfer coefficient [15].

Continuity equations for the coolant:

$$\frac{\partial u}{\partial x} + \frac{\partial v}{\partial y} + \frac{\partial w}{\partial z} = 0 \tag{1}$$

Momentum equations:

$$\rho_f \left( \frac{\partial (uu)}{\partial x} + \frac{\partial (uv)}{\partial y} + \frac{\partial (uw)}{\partial z} \right) = -\frac{\partial p}{\partial x} + \mu_f \left( \frac{\partial}{\partial x} \left( \frac{\partial u}{\partial x} \right) + \frac{\partial}{\partial y} \left( \frac{\partial u}{\partial y} \right) + \frac{\partial}{\partial z} \left( \frac{\partial u}{\partial z} \right) \right) + \rho f_x \tag{2}$$

$$\rho_f \left( \frac{\partial (uv)}{\partial x} + \frac{\partial (vv)}{\partial y} + \frac{\partial (vw)}{\partial z} \right) = -\frac{\partial p}{\partial y} + \mu_f \left( \frac{\partial}{\partial x} \left( \frac{\partial v}{\partial x} \right) + \frac{\partial}{\partial y} \left( \frac{\partial v}{\partial y} \right) + \frac{\partial}{\partial z} \left( \frac{\partial v}{\partial z} \right) \right) + \rho f_y$$
(3)

$$\rho_f \left( \frac{\partial (uw)}{\partial x} + \frac{\partial (wv)}{\partial y} + \frac{\partial (ww)}{\partial z} \right) = -\frac{\partial p}{\partial z} + \mu_f \left( \frac{\partial}{\partial x} \left( \frac{\partial w}{\partial x} \right) + \frac{\partial}{\partial y} \left( \frac{\partial w}{\partial y} \right) + \frac{\partial}{\partial z} \left( \frac{\partial w}{\partial z} \right) \right) + \rho f_z \tag{4}$$

Energy equation in fluid domain is shown as:

$$\rho_f C_{p,f} \left( u \frac{\partial T_f}{\partial x} \right) + \left( v \frac{\partial T_f}{\partial y} \right) + \left( w \frac{\partial T_f}{\partial z} \right) = k_f \left( \frac{\partial^2 T_f}{\partial x^2} + \frac{\partial^2 T_f}{\partial y^2} + \frac{\partial^2 T_f}{\partial z^2} \right), \tag{5}$$

and for solid domain is written as:

$$k_s \left( \frac{\partial^2 T_s}{\partial x^2} + \frac{\partial^2 T_s}{\partial y^2} + \frac{\partial^2 T_s}{\partial z^2} \right) = 0 \tag{6}$$

## 2.4 Boundary Conditions

The flow type in the minichannel is modelled by imposing appropriate boundary conditions. This is to obtain an accurate CFD solution that reflects the real condition as in the experimental work. The boundary conditions specify the fluid behaviour at the boundaries of the whole domain.

#### 2.4.1 Velocity inlet

The fluid enters the computational domain through the inlet face. The incoming flow is assumed to be constant at a specified temperature as the experimental value. The coolant velocity at all fluid-solid boundaries is assumed to be equal to the solid boundary and this applies to the no-slip condition. The inlet velocity in radial and transverse direction is assumed to be zero and only tangential velocity acting on the inlet surface as in Eq. (7). The inlet velocity is calculated at a certain Reynolds number as in Eq. (8).

$$u_{x=0} = u_{in}, \ v_{x=0} = 0, \ w_{x=0} = 0, \ T_{x=0} = T_0$$
 (7)

$$u_{in} = \frac{Re\mu}{\rho D_h} \tag{8}$$

# 2.4.2 Wall boundary

There are three types of wall boundaries. First, the heat flux at the bottom of the heat sink is assumed to spread equally. Since the energy equation is solved, the heat flux from the heater is shown in Eq. (9) and the amount of heat absorbed by the fluid from the wall through conduction is calculated using Eq. (10).

$$q_{bottom} = k_s \frac{\partial T_s}{\partial z} \tag{9}$$

$$q_f = m_f c_p dT (10)$$

The coupled wall is imposed on the faces inside the computational domain which defined the solid-fluid interface. The solid-fluid interface wall receives heat transfer from the wall through conduction using Eq. (11).

$$q_{interface} = k_s \frac{\partial T_s}{\partial z} \tag{11}$$

The outer surrounding of the heat sink is wrapped with a rock wool. Hence, the wall surrounding the model is assumed to be adiabatic as shown in Eq. (12) as no heat flows in and out of the boundary.

$$\frac{\partial T_s}{\partial z} = 0 \tag{12}$$

## 2.4.3 Outlet boundary

The pressure out of the computational domain is set to be the same as atmospheric pressure, and being set at the channel outlet.

#### 2.4.4 Internal boundary

The interior boundary conditions are specified at the faces that are formed in between several multi blocks within the computational domain. There are flows crosses through these faces as the fluid flows across the cells. This is to ensure connections between the multi blocks.

#### 2.4.5 Thermophysical properties

The thermophysical properties of the coolant fluid in this study are assumed to be constant and shown in Table 2.

**Table 2**Thermal properties of fluids at T = 300K

Coolant	$\rho$ (kg/m <sup>3</sup> )	k (W/mK)	$c_{\rho}(J/kgK)$	μ (Ns/m²)
Propylene Glycol Water, pgw	1010.0000	0.45200	3939.194	0.00076714

# 2.4.6 Grid independence test

The grid independence test is done by changing the global mesh size and the suitable mesh size is selected at which Nusselt number variation is minimized and approaches constant as the mesh size is varied. The difference of Nusselt number value for very coarse grid to a very fine grid is less than 3% even though there is a bump in Nusselt number value for conventional microchannel heat sink. This shows that the very coarse grid is acceptable in predicting the Nusselt number. From this test, the optimum mesh size is chosen for the whole domain which refers to 341531, 408340 and 585153 number of cells for conventional, design A and design B type while mesh size of 120 x 100 x 21 for

682825 number of cells for design C type. Figure 5 shows the mesh used for all type of heat sink for minichannel.

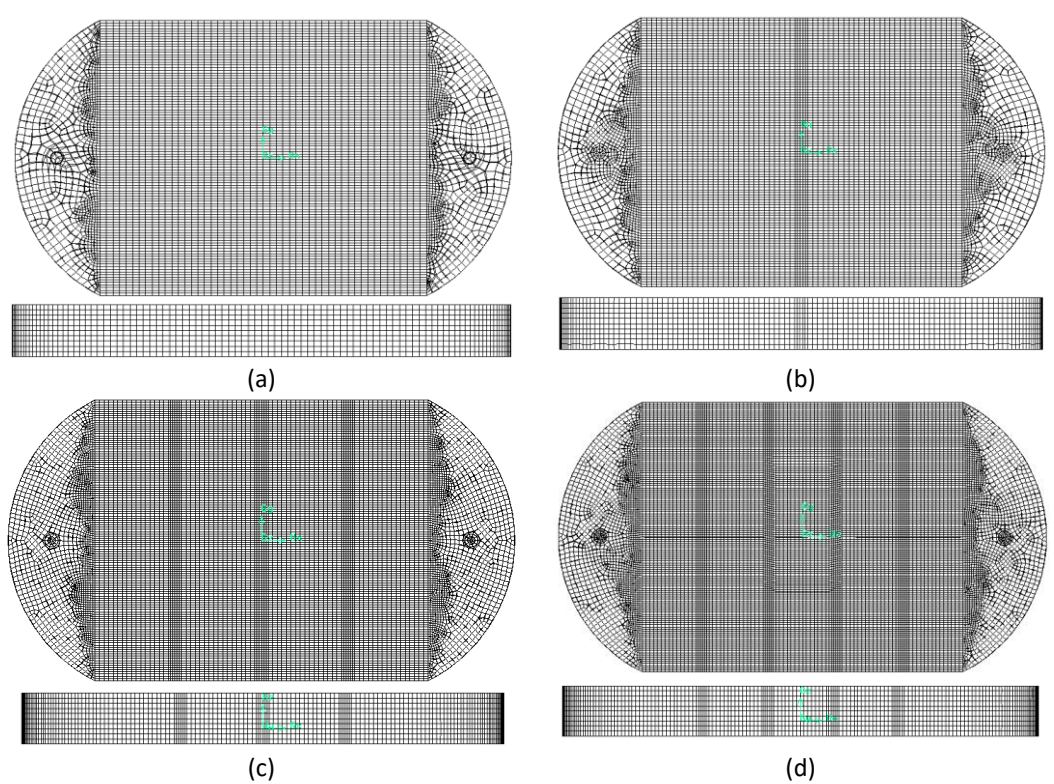


**Fig. 5.** The meshed domain for (a) straight, (b) design A, (c) design B and (d) design C type heat sink

#### 2.4.7 Convergence

The CFD is run using double precision for all cases to obtain high precision in the CFD solution. The governing equations are solved until convergence is attained. Residuals below  $10^{-6}$  are obtained to minimize deviations of the CFD solutions with the true value.

# 2.4.8 Postprocessing

The final step in numerical work is how the results of the determined parameters are extracted using mass-weighted averaging technique. The mass-weighted average of a quantity is computed on the surfaces of interest such as the local temperature and pressure on the fluid domain, while the heat flux and wall shear stress are computed on the wall surface.

The variable properties that are used to predict the fluid and thermal flow are outlet temperature,  $T_{out}$ , inlet temperature,  $T_{in}$ , mean temperature,  $T_{m}$ , wall temperature,  $T_{wall}$ , and heat flux, q''. For validation purpose, some of the variables are taken at the same point as in the experimental work. For  $T_{out}$  and  $T_{in}$ , these values are computed through mass-weighted averaging performed on the outlet and inlet surface.  $T_{m}$  is calculated based on Eq. (13).

$$T_m = \frac{T_{in} + T_{out}}{2} \tag{13}$$

The heat flux, q'' is defined as the heat absorbed to the fluid and is represented as Eq. (14).

$$q'' = mc_p(T_{out} - T_{in}) \tag{14}$$

Meanwhile, the heat transfer coefficient and Nusselt number are calculated as in Eq. (15) and Eq. (16) respectively.

$$h = \frac{q''}{\Delta T} = \frac{q''}{T_W - T_m} \tag{15}$$

$$Nu = h \, x \, \frac{D_h}{k} \tag{16}$$

For variable properties, computed values are taken along the surface of the targeted region. For example, the local temperature, velocity and pressure distribution are computed at the centerline of the channel. Meanwhile, the wall stress shear is computed on the centerline of the channel's bottom wall. Some of the local predicted properties are computed on the side wall, bottom wall or mean line of the channel as shown in Figure 6.

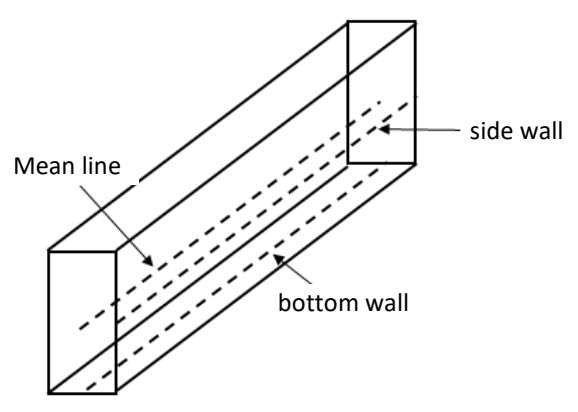


**Fig. 6.** Lines of side wall, bottom wall and middle line shows the location of computed predicted data for a single channel

#### 3. Results

This section portrays the simulated results that includes the validation part and the predetermined output parameters.

## 3.1 Validation

The numerical data is compared to experimental data for validation purposes. The length ratio,  $L_c/L_{ch}$  of 0, 0.08333, 0.181818 and 0.238095 are correspondingly referred to straight, design A, design B and design C minichannel type as shown in Table 1. In this study, the deviation of  $P_{drop}$ , and Nusselt number as in Figure 7 and Figure 8 lies from 0.49% to 9.81%, and 1.08% to 12.48% respectively. Some of these experimental data may be under-predicted or over-predicted the experimental data due to uncontrolled environment temperature.

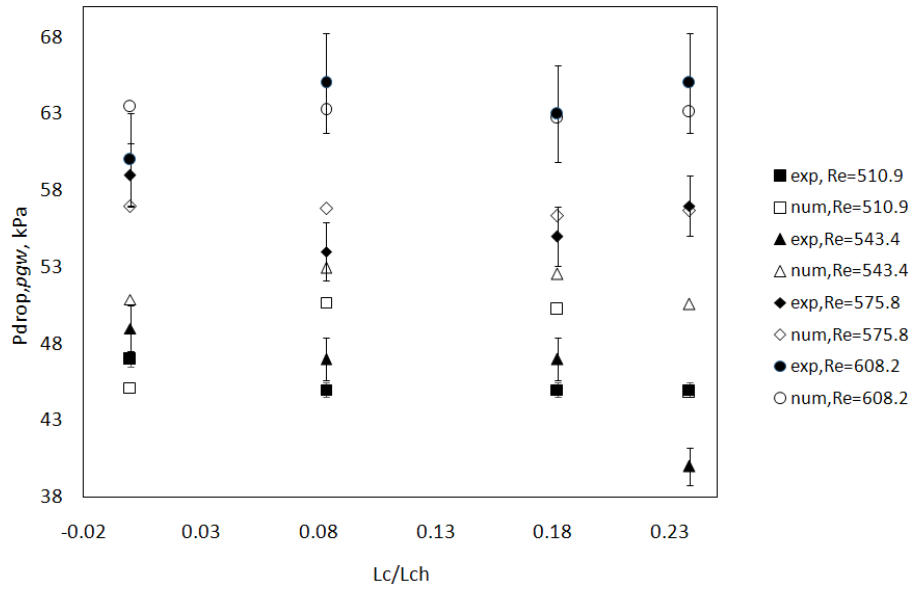
Referring to Figure 7, the pressure drop occurs within the channel is due to friction losses along the channel, losses in manifold and losses in bend areas. The variation in pressure drop for propylene glycol-water is observed as much as 17%. The pressure losses depend much on the Reynolds number of the flow. With the same Reynolds number, the ratio of kinematic viscosity to the density (or kinetic

viscosity) of fluid very much affects the velocity distribution between the inlet and outlet of a minichannel heat sink. This ratio affects the velocity distribution in the fluid and results in pressure drop variation. As shown in Figure 7, some discrepancies exist between numerical and experimental data. At the mini-scale, the surface forces become dominant which affect much in experimental data and overpredicted the pressure drop. Besides, the geometry deviations of the actual heat sink are sensitive due to manufacturing tolerances, edge imperfections and unsmooth surface roughness. All this causes underpredicted and overpredicted pressure drop.

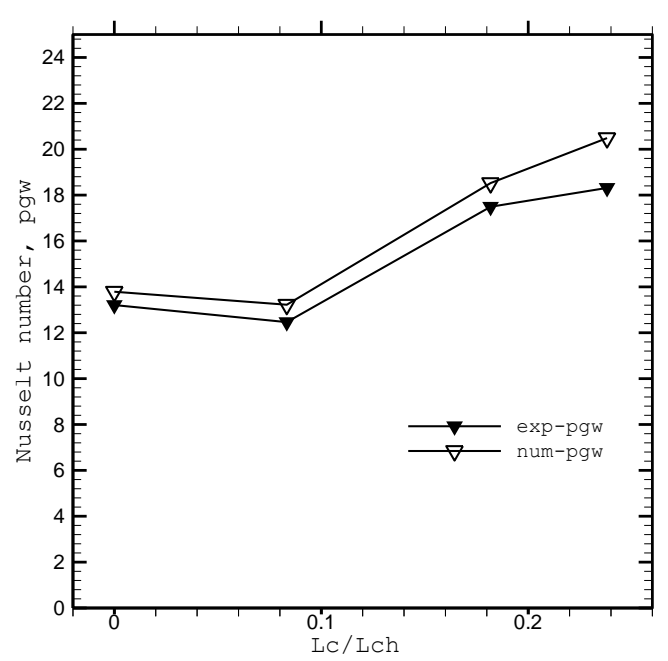
As the velocity increases, the temperature difference between the outlet and inlet heat sink decreases and the heat absorbed by the fluid increases. This leads to the increment in heat transfer and Nusselt number as shown in Figure 8. The average Nusselt number for all fluid depends on the channel's design, and the ratio of specific heat to thermal conductivity, of fluid. Besides, the variation of Nusselt number for each fluid is also affected due to minichannel configuration which will be discussed further.

A correlation displayed in Eq. (17) shows the Nusselt number of a fully developed laminar flow in rectangular ducts with constant heat flux condition, which is 3.99 [20]. Using this equation, the Nusselt number for fully developed flow for straight microchannel in this study is approximately 5.815. At the same aspect ratio of 4 which equivalent to height to width ratio,  $\alpha$  as in this study, the Nusselt number is predicted as 5.33 [21].

$$Nu = 8.235(1 - 1.883\alpha + 3.767\alpha^2 - 5.814\alpha^3 + 5.361\alpha^4 - 2\alpha^5)$$
(17)



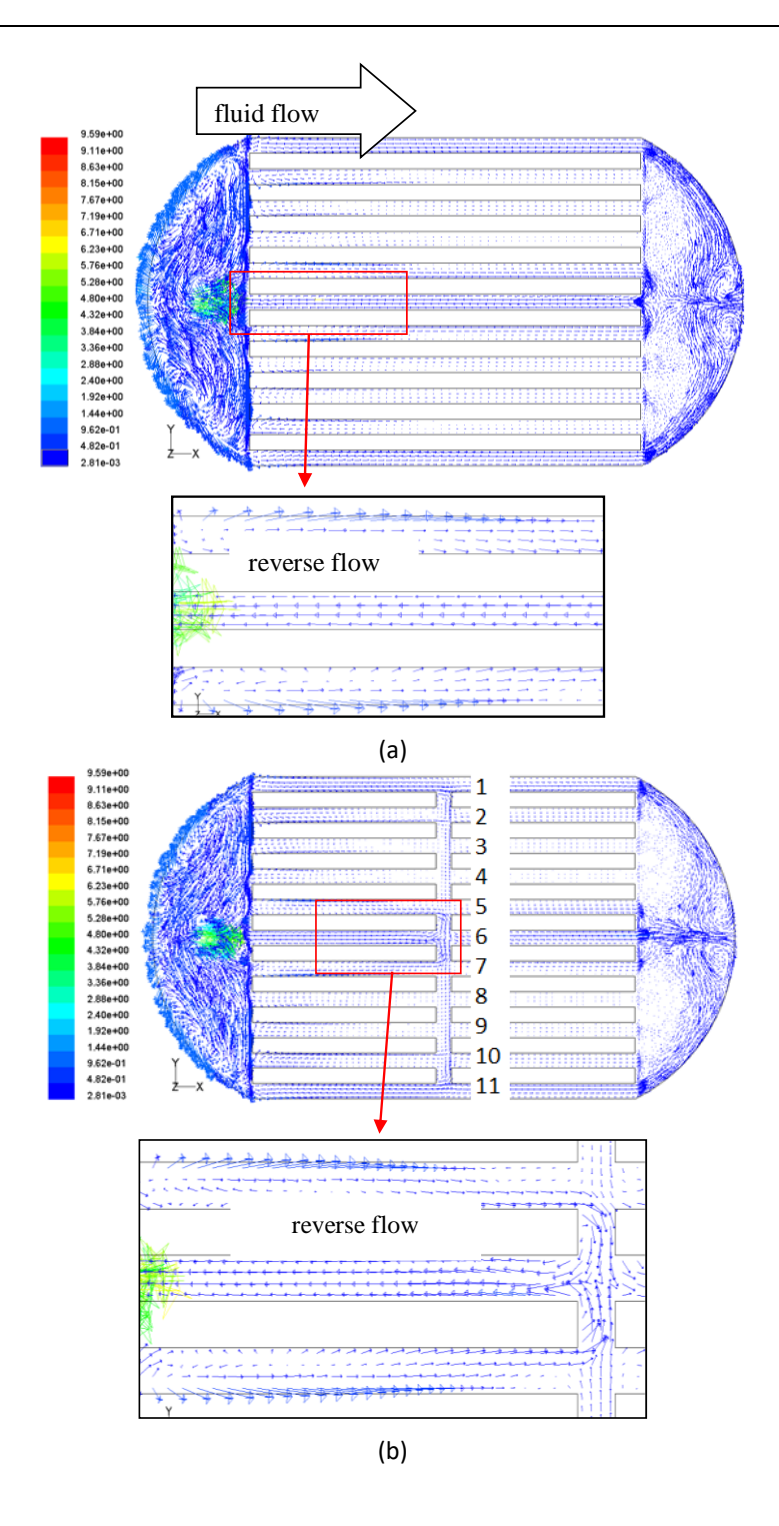
**Fig. 7.**  $P_{drop}$  of experimental and numerical for straight and interrupted minichannel heat sink using propylene glycol water at various Reynolds number



**Fig. 8.** Average Nusselt number of experimental and numerical for straight and interrupted minichannel heat sink using propylene glycol-water at  $Re_{ch}$ =510.9

# 3.2 Velocity Vector

Figure 9 shows the velocity vectors of propylene glycol-water mixture in all type of minichannel heat sink. High flow rate is observed in channels 5 and 7 as in Figure 9(b) causes some of propylene glycol water to splatter off in the direction of the flow and some reverse back into channel no 6. All minichannels show high flow in channel number 1, 2, 5-7, 10 and 11. Lower flow distribution occurs in the rest of channels. This is because very high flow from the main inlet circulates and cannot be distributed evenly among all channels. A sharp-edge inlet of each channel separates the flow from the left manifold. Very high velocity in the left manifold due to accumulated fluid volume is forced to flow into minichannels that have very high difference inlet in hydraulic diameter. This sharp-edge inlet channel acts as a constriction which decreases the flow area and causes a great loss. This results in very low velocity in each channel's inlet.



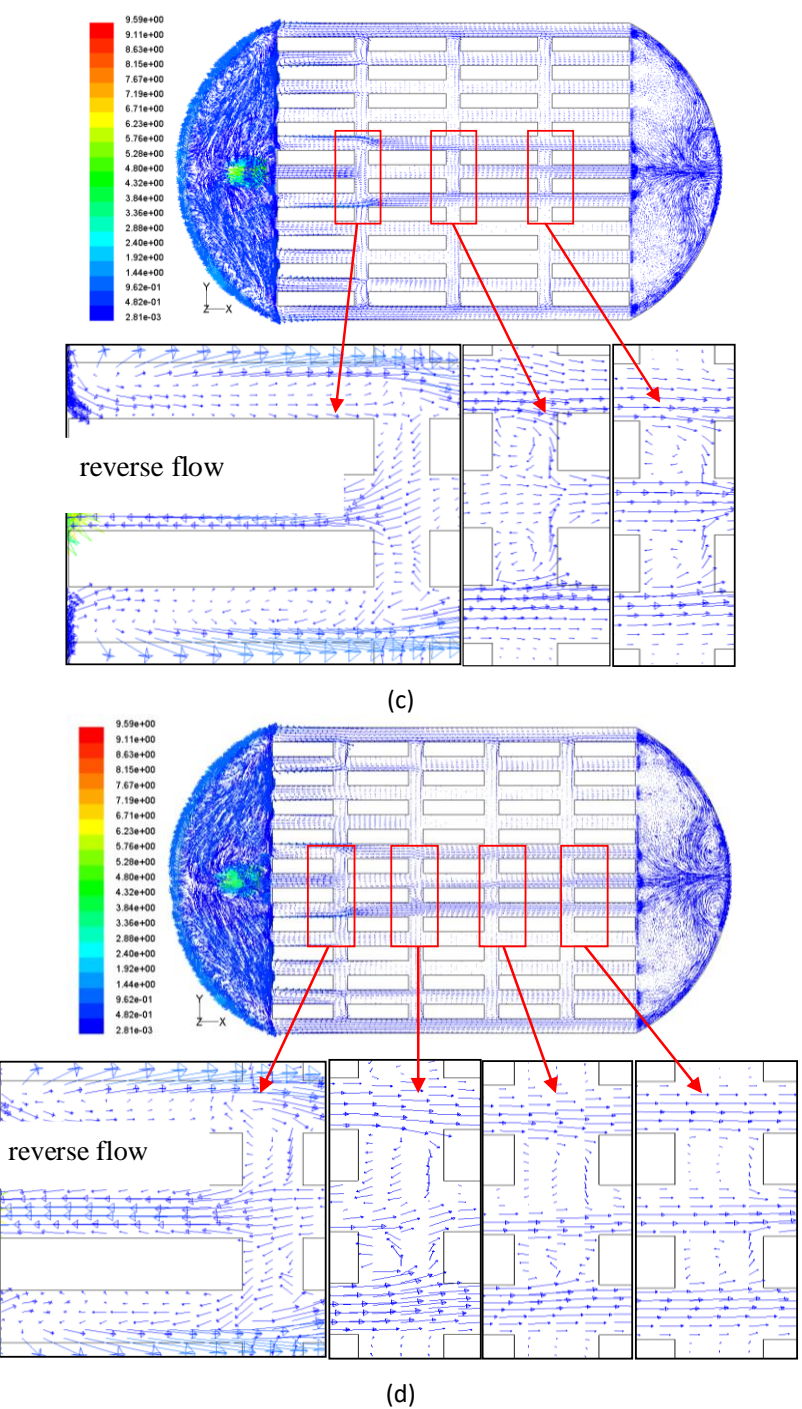


**Fig. 9.** Velocity vector of propylene glycol-water for (a) straight, (b) design A, (c) design B and (d) design C type minichannel type

At each of sharp-edge of cut section, the Coanda effect is avoided to occur. This phenomenon occurs when the fluid which is initially cling to the solid body surface after high velocity from the inlet being separated from the wall surface and induces the swirling flow. This promotes the fluid circulation and flow separation as in as in Figure 10 at each bend or curve that leads to stagnant flow or low velocity region and yields drops in pressure [22]. Even though the losses might be very small and negligible in most high Reynolds number cases, this is significant in this study which deals with laminar and low Reynolds number. As the fluid flows along the channels, the magnitude of the velocity decreases due to friction along the channel surface. As there are more cut sections formed in each channels, the magnitude of circulation becomes smaller and lower the fluid mixing.

Higher velocity due to accumulation of fluid at the inlet and outlet are observed in conserving the constant mass flow rate throughout the control surface of each domain. In the direction of fluid flow (to the right), the control surface becomes wider and the velocity gradually decrease towards the end of the channel while increasing back and accumulated at the outlet manifold.

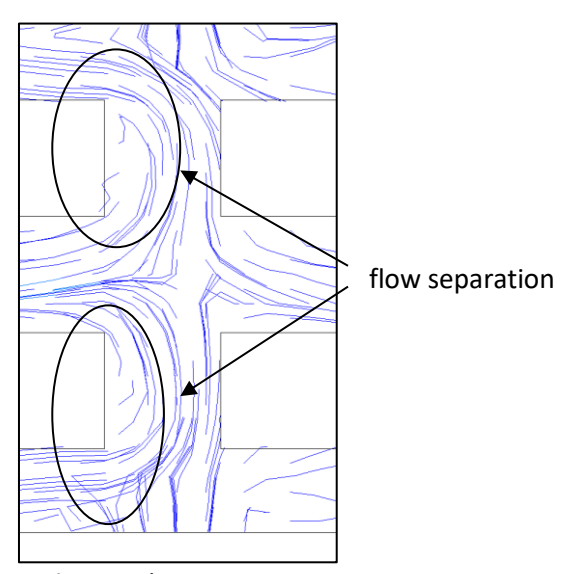


Fig. 10. Flow separation at cut section area

#### 3.3 Heat Flux

Figure 11 shows the local heat flux computed on the side wall and bottom wall of the channel for all types of minichannel. As the fluid flows along the channel, the fluid temperature near the wall becomes hot. Hence, the temperature difference of the wall and the fluid temperature becomes higher. At the cut sections, there is a sudden drop of heat flux, which nearly approaches zero as in Figure 11(a). There is no wall in this region, except for flowing fluid. Comparing the heat flux between all types of minichannels, the heat flux starts to decrease and increase back at the inlet and outlet of cut section respectively. This happens because the velocity increases and decreases while disturbs the velocity gradient. At each of cut section, lower velocity yields higher temperature and heat flux approaches zero because there is no wall on the side channel as in Figure 11(a). This causes shorter thermal entrance length [23].

Figure 11(b) shows the wall heat flux at the bottom wall of the channel. It directly influences the overall heat transfer process in a microchannel heat sink. The bottom heat flux is increasing along the channel. There are several bumps of heat flux value according to the number of cut section. A higher heat flux implies a greater amount of heat energy being transferred through a given area. This necessitates a stronger driving force for heat transfer, such as a larger temperature difference between the heat source at the bottom wall and the fluid.

At each of cut section, velocity of fluid is lower. Hence, it causes lower fluid temperature in that area. This results in higher temperature differences between the wall and fluid interface near the wall and leads to higher heat flux in each cut section area. The heat transfers continuous to occur as the heat flux increases, showing there exists temperature differences between cold fluid and the hot wall. No thermal equilibrium is attained since the bottom heat flux is continuously increasing until the end of the channel. The highest heat flux at the side and bottom wall is attained in design C with the use of propylene glycol-water.

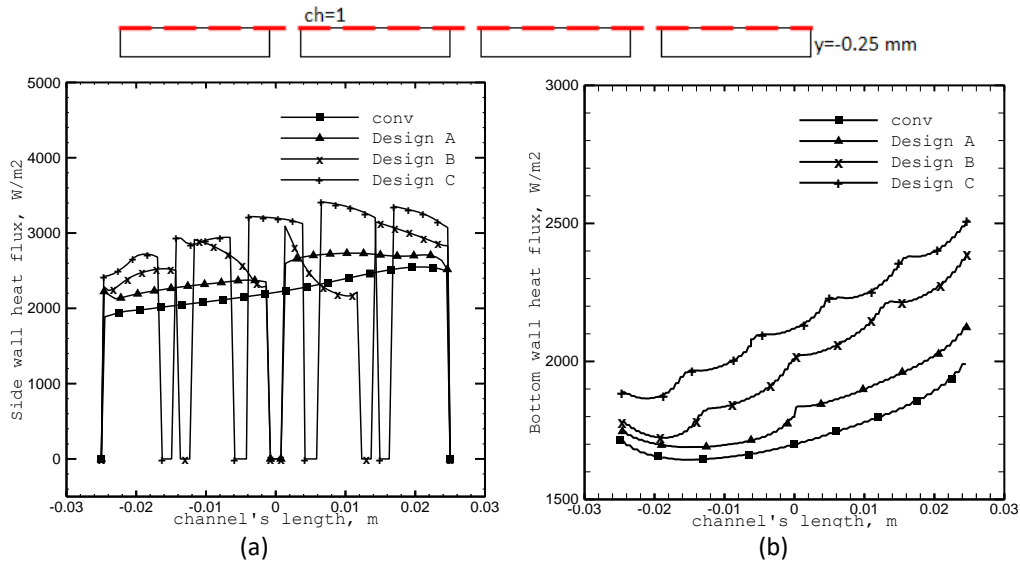


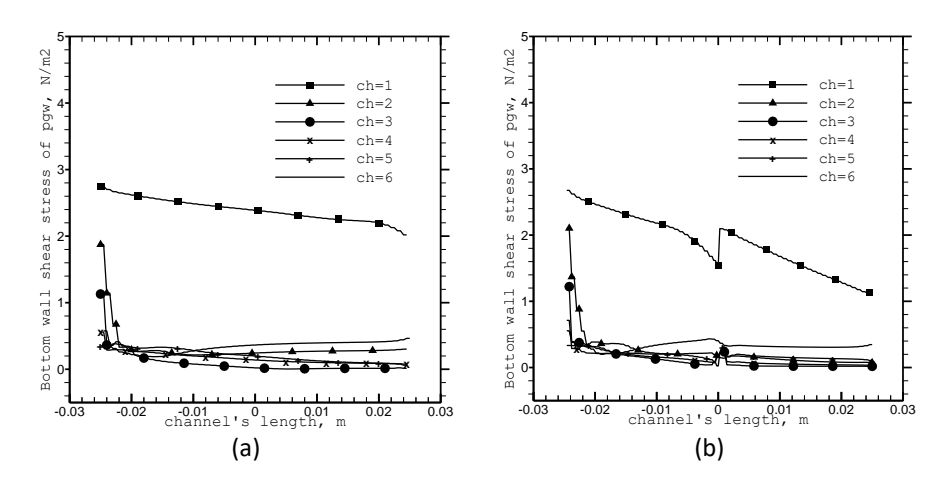
**Fig. 11.** Local heat fluxes (a) on side wall and (b) bottom wall for propylene glycolwater at Re=510.9

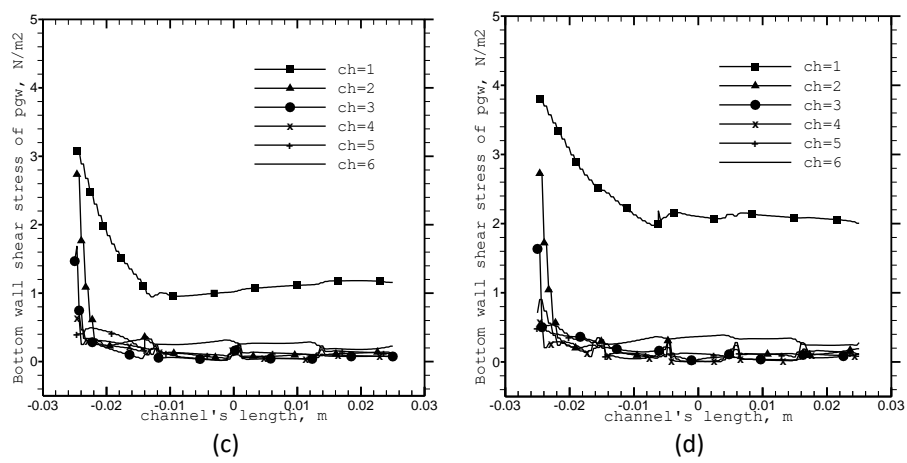
#### 3.4 Wall Shear Stress

Figure 12 shows the bottom wall shear stress for all type of minichannel heat sink. The highest wall shear stress is depicted in the middle channel since the fluid flows with the highest velocity in this channel. The velocity gradient is the highest in design C shows the highest heat transfer rate in the minichannel. At each cut section, the wall shear stress is fluctuated due to variations in velocity gradient as the fluid flows along the channel.

The temperature ratio as shown in Figure 13 explains the behaviour of heat transfer coefficient. The highest heat transfer coefficient is attained in design C type minichannel with the highest temperature ratio of 0.52. High irregular flow in design C type as compared to other design due to number of cut section as observed in other work of Dang *et al.*, [24] causes high fluctuation in local velocity that affects the temperature ratio.

Higher wall shear stress lead to increased turbulence and mixing within the fluid, while corresponds to a thinner boundary layer and resulting in improved heat transfer coefficients. This is particularly evident in microchannels with complex geometries. While increased wall shear stress improves heat transfer, it also contributes to higher pressure drop.





**Fig. 12.** Wall shear stress at bottom of channel for (a) straight, (b) design A, (c) design B, and (d) design C of minichannel heat sink for propylene glycol water at  $Re_{ch}$ =510.9

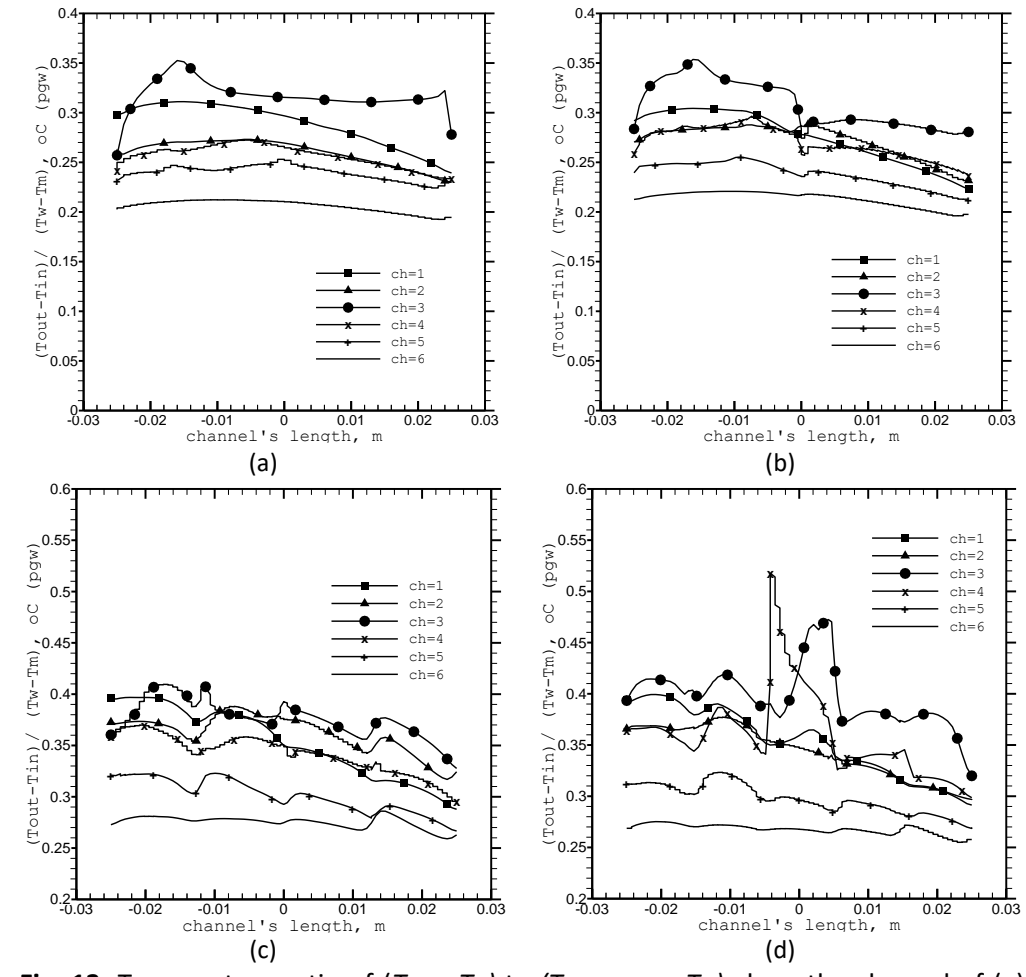


**Fig. 13.** Temperature ratio of  $(T_{out} - T_{in})$  to  $(T_{bottom\ wall} - T_m)$  along the channel of (a) straight, (b) design A, (c) design B and (d) design C type minichannel heat sink at  $Re_{ch}$ =510.9

Although a range of Reynolds numbers was investigated in the simulations, more research is necessary to see whether this result can be applied to higher Reynolds number. Higher flow regimes could cause flow instabilities or change the reported improvements in heat transfer in practical applications.

Besides, the simulations were conducted using water, propylene glycol-water, and *ZnO*-water limiting the generalizability of the findings to other coolants. Different fluids possess varying thermophysical properties that could impact the flow dynamics and heat transfer characteristics. Studies employing other coolants would be necessary to assess the broader applicability of the interrupted minichannel designs.

In addition to that, the idealized channel geometry was assumed in the simulations. However, in a real-world fabrication, manufacturing flaws like surface roughness, dimensional variances, or irregularities in the cut geometries are unavoidable. These flaws may greatly impact the performance of heat transfer and flow patterns. To measure the effect of manufacturing tolerances on the effectiveness of the interrupted minichannel designs, more research is required.

#### 4. Conclusions

A computational fluid dynamics (CFD) study was conducted to assess the performance of interrupted minichannel heat sinks as compared to a straight channel design. The interrupted minichannles here refers to some cuts in between the straight channel. Four minichannel configurations; a straight channel and three interrupted designs (A, B, and C) were examined. All channels had a rectangular cross-section with a hydraulic diameter of 0.032 m and incorporated cuts. Parametric analyses were performed using propylene glycol-water mixture as coolants, with Reynolds numbers ranging from 510.9 to 608.2. The flow was modeled as steady and threedimensional flow. Model validation against experimental data for pressure drop and Nusselt number yielded deviations of 0.49% to 9.81% and 1.08% to 12.48%, respectively for distilled water and propylene glycol-water mixture. Simulation results indicated that design features, such as sharp corners at every cuts part, influenced flow behavior by inducing flow separation, recirculation, and boundary layer disruption. Comparative analysis showed that the increment in heat flux by 26.3% to 33.3%,  $(T_{out}-T_{in})/(T_w-T_m)$  by 25% to 42.8%, and decrement in wall shear stress by 25% to 35.7% as compared to straight minichannel heat sink. All these indicates the increment in heat transfer within each channel which will be investigated for further study. Apart from that, the interrupted minichannel heat sink outperform the straight channel based on the parametric studies done and design C outperform the other designs. The flow behaviors such as flow separation, reverse flow, recirculation zones, and boundary layer interruption are caused by the interrupted designs. These designs are effectively responsible for disrupting the thermal boundary layer, promoting enhanced heat transfer.

### **Authors Contribution**

Ernie Mat Tokit: Writing – concepts-original draft & review. Mohd Zamri Yusoff: Writing and Review. Safarudin Gazali Herawan: some of data collection and analysis, & review.

# **Data Availability**

https://zenodo.org/records/14955092

#### Acknowledgement

This research was not funded by any grant. The resources and assistance received in completing this work have been generously provided by Universiti Teknikal Malaysia Melaka and Universiti Tenaga Nasional.

#### References

- [1] Everts, Marilize, and Faiyaad Mahomed. "The effect of high values of relative surface roughness on heat transfer and pressure drop characteristics in the laminar, transitional, quasi-turbulent and turbulent flow regimes." *Heat and Mass Transfer* 60, no. 7 (2024): 1173-1193. https://doi.org/10.1007/s00231-024-03472-1
- [2] Saadoon, Zahraa H., Farooq H. Ali, Hameed K. Hamzah, Azher M. Abed, and M. Hatami. "Improving the performance of mini-channel heat sink by using wavy channel and different types of nanofluids." *Scientific Reports* 12, no. 1 (2022): 9402. https://doi.org/10.1038/s41598-022-13519-0
- [3] Ahmadi, A., A. A. Ranjbar, M. J. Hosseini, and Y. Pahamli. "Improvement of mini-channel heat sink using thin-wall fins." *Journal of the Brazilian Society of Mechanical Sciences and Engineering* 45, no. 10 (2023): 532. https://doi.org/10.1007/s40430-023-04353-0
- [4] Panitz, T., and D. T. Wasan. "Flow attachment to solid surfaces: the Coanda effect." *AIChE Journal* 18, no. 1 (1972): 51-57. <a href="https://doi.org/10.1002/aic.690180111">https://doi.org/10.1002/aic.690180111</a>
- [5] Tuckerman, David Bazeley. *Heat-transfer microstructures for integrated circuits (cooling, heat-sink)*. Stanford University, 1984.
- [6] Zhao, Qianbin, Dan Yuan, Jun Zhang, and Weihua Li. "A review of secondary flow in inertial microfluidics." *Micromachines* 11, no. 5 (2020): 461. <a href="https://doi.org/10.3390/mi11050461">https://doi.org/10.3390/mi11050461</a>
- [7] Mamidi, Nitin Kumar, Karthik Balasubramanian, Kiran Kumar Kupireddi, Chandramohan V. P., Yash Kishor Kumar Sahu, and Pallikonda Mahesh. "Influence of secondary flow channels on heat transfer and fluid flow characteristics in curved microchannel." *Asia-Pacific Journal of Chemical Engineering* 17, no. 6 (2022): e2833. https://doi.org/10.1002/apj.2833
- [8] Cengel, Yunus, and John Cimbala. *Ebook: Fluid mechanics fundamentals and applications (si units)*. McGraw Hill, 2013.
- [9] Fan, Liang-Liang, Xu-Kun He, Yu Han, Li Du, Liang Zhao, and Jiang Zhe. "Continuous size-based separation of microparticles in a microchannel with symmetric sharp corner structures." *Biomicrofluidics* 8, no. 2 (2014). <a href="https://doi.org/10.1063/1.4870253">https://doi.org/10.1063/1.4870253</a>
- [10] Joseph, Jojomon, Danish Rehman, Michel Delanaye, Gian Luca Morini, Rabia Nacereddine, Jan G. Korvink, and Juergen J. Brandner. "Numerical and experimental study of microchannel performance on flow maldistribution." *Micromachines* 11, no. 3 (2020): 323. <a href="https://doi.org/10.3390/mi11030323">https://doi.org/10.3390/mi11030323</a>
- [11] Fung, Chang Kai, and Mohd Fadhil Majnis. "Computational fluid dynamic simulation analysis of effect of microchannel geometry on thermal and hydraulic performances of micro channel heat exchanger." *Journal of Advanced Research in Fluid Mechanics and Thermal Sciences* 62, no. 2 (2019): 198-208.
- [12] Nadaraja, Darvind, Natrah Kamaruzaman, Ummikalsom Abidin, and Mohsin Mohd Sies. "Experimental study on the effect of multilayer microchannel arrangement to the thermal hydraulic performance of microchannel arrays." *Journal of Advanced Research in Fluid Mechanics and Thermal Sciences* 57, no. 1 (2019): 23-31.
- [13] Zahmani, Qamar Fairuz, Muhammad Nur Othman, Mohd Faruq Abdul Latif, Siti Nor'ain Mokhtar, Nik Nazri Nik Ghazali, and Ahmad Yusof Ismail. "Numerical heat transfer analysis in microchannel heat sink with different aspect ratio." *Journal of Advanced Research in Fluid Mechanics and Thermal Sciences* 62, no. 2 (2019): 265-273.
- [14] Soundrapaman, Allison, Normayati Nordin, Abdoulhdi A. Borhana Omran, and Abdulhafid M. A. Elfaghi. "Numerical Investigation of Heat Transfer Enhancement of Al<sub>2</sub>O<sub>3</sub> Nanofluid in Microchannel Heat Sink." *Journal of Advanced Research in Fluid Mechanics and Thermal Sciences* 107, no. 1 (2023): 19-28. https://doi.org/10.37934/arfmts.107.1.1928
- [15] Bhandari, Prabhakar, Kamal S. Rawat, Yogesh K. Prajapati, Diwakar Padalia, Lalit Ranakoti, and Tej Singh. "A review on design alteration in microchannel heat sink for augmented thermohydraulic performance." *Ain Shams Engineering Journal* 15, no. 2 (2024): 102417. https://doi.org/10.1016/j.asej.2023.102417
- [16] Singh, Shashank, Anup Malik, and Harlal Singh Mali. "A critical review on single-phase thermo-hydraulic enhancement in geometrically modified microchannel devices." *Applied Thermal Engineering* 235 (2023): 121729. <a href="https://doi.org/10.1016/j.applthermaleng.2023.121729">https://doi.org/10.1016/j.applthermaleng.2023.121729</a>
- [17] Japar, Wan Mohd Arif Aziz, Nor Azwadi Che Sidik, Siti Rahmah Aid, Yutaka Asako, and Tan Lit Ken. "A comprehensive review on numerical and experimental study of nanofluid performance in microchannel heatsink (MCHS)." *Journal of Advanced Research in Fluid Mechanics and Thermal Sciences* 45, no. 1 (2018): 165-176.
- [18] Loon, Yew Wai, Nor Azwadi Che Sidik, and Yutaka Asako. "Numerical Analysis of Fluid Flow and Heat Transfer Characteristics of Novel Microchannel Heat Sink." *Journal of Advanced Research in Numerical Heat Transfer* 15, no. 1 (2023): 1-23. https://doi.org/10.37934/arnht.15.1.123
- [19] Rohaizan, Muhammad Hazeer Khiralsaleh Mohamad, Nor Azwadi Che Sidik, and Kamyar Shameli. "Numerical Analysis of Heat Transfer in Microchannel Heat Transfer in Microchannel Heat Sink using Flow Disruption." *Journal of Advanced Research Design* 106, no. 1 (2023): 1-13. https://doi.org/10.37934/ard.106.1.113

- [20] Kays, William M., and Michael E. Crawford. Convective heat and mass transfer. McGraw-Hill, 1993.
- [21] Shah, R. K., and Alexander Louis London. *Laminar flow forced convection in ducts: a source book for compact heat exchanger analytical data*. Academic Press, 1978.
- [22] Xia, Guodong, Lei Chai, Mingzheng Zhou, and Haiyan Wang. "Effects of structural parameters on fluid flow and heat transfer in a microchannel with aligned fan-shaped reentrant cavities." *International Journal of Thermal Sciences* 50, no. 3 (2011): 411-419. <a href="https://doi.org/10.1016/j.ijthermalsci.2010.08.009">https://doi.org/10.1016/j.ijthermalsci.2010.08.009</a>
- [23] Lee, Poh-Seng, and Suresh V. Garimella. "Thermally developing flow and heat transfer in rectangular microchannels of different aspect ratios." *International Journal of Heat and Mass Transfer* 49, no. 17-18 (2006): 3060-3067. https://doi.org/10.1016/j.ijheatmasstransfer.2006.02.011
- [24] Dang, Minh, Ibrahim Hassan, and Sung In Kim. "Numerically investigating the effects of cross-links in scaled microchannel heat sinks." Journal of Fluids Engineering 130, no. 12 (2008): 121103. https://doi.org/10.1115/1.3001093